Green Chemistry

PAPER

View Article Online
View Journal | View Issue

Cite this: *Green Chem.*, 2023, **25**, 8808

Sonochemical oxidation of technical lignin to obtain nanoparticles with enhanced functionality†

Nagore Izaguirre,[a] Javier Fernández-Rodríguez,[a] Eduardo Robles[b] and Jalel Labidi *[a]

Kraft lignin (KL) was treated by employing mild oxidation conditions enhanced by ultrasound irradiation (US) for obtaining more functionalized particles, avoiding the undesired side reactions of degradation and depolymerization. The aim was to obtain products with plausible value for applications with a greater potential market, enabling the introduction of low-cost bio-based materials for technically advanced applications. In the present work, KL was oxidized in alkaline media, applying low temperatures (30–60 °C), short times (15 to 60 min), and US waves (20 kHz). The influence of incorporating hydrogen peroxide (H_2O_2) as an oxidizing agent was also studied, as well as the chemical composition, physico-chemical, thermal, and morphological properties of the final lignin particles. It was observed from Quantitative Acid Hydrolysis (QAH), Elemental Analysis (EA), and molecular weights (M_w) that oxidized lignin particles (OxL) did not suffer any major degradation. Other techniques used to determine physico-chemical properties, such as Fourier Transformed Infrared (FTIR), 31 Phosphorous Nuclear Magnetic Resonance (^{31}P NMR), or Ultraviolet–visible (UV-vis) methods, corroborated oxidation reactions, evident by the increment of carboxylic groups. The most noticeable difference, however, was observed when the stability and morphology of the particles were observed by Dynamic Light Scattering (DLS) and Transmission Electron Microscopy (TEM). Some conditions greatly promoted the formation of more stable and nanosized particles. The best conditions were the mildest but with the highest reaction times (no addition of H_2O_2, 30 °C and 60 minutes). Moreover, all reactions had good recovery yields, above 70% of the original lignin.

Received 30th March 2023,
Accepted 21st September 2023

DOI: 10.1039/d3gc01037f

rsc.li/greenchem

Introduction

Biorefineries are essential tools for the transition of more efficient and sustainable development, able to substitute petroleum-based products with biomass-derived products.[1] Lignin has been addressed as a key compound for biorefinery development and forest-based circular bioeconomy.[2] It has been widely studied for various applications since it is a major component of wood and the most abundant aromatic biopolymer. Nevertheless, its commercial and economic perspectives demand different approaches to large-scale valorization. Recent progress in the development of novel, greener biorefinery processes have been carried out, where not only more sustainable solvents like Ionic Liquids and Deep Eutectic Solvents have been implemented,[3] but also lignin transformation and modification processes have been designed for further valorization in high value-added products. Processes like depolymerization, pyrolysis, and hydroprocessing have been widely explored, along with ultrafiltration, selective pH precipitation, mechanical membrane filtration, and fractionation utilizing green solvents.[4] One of the most studied strategies for lignin valorization has been its oxidation, a route to obtain smaller molecules, such as aromatic aldehydes (vanillin being industrially manufactured), ketones, and acids.[5–7] By the cleavage of the inter-unit linkages in the lignin molecule, its potential to replace current marketed aromatic compounds from fossil resources has drastically increased. Moreover, the obtaining of these molecules, more homogeneous than their predecessor and highly functionalized due to the increment in reactive functional groups, ease their application as building-block compounds for value-added markets,[8] such as adhesives,[9] thermosetting polyester coatings,[10] nanocarriers for drug delivery,[11] antioxidant/antimicrobial agents, light-harvesting complexes, environmental remediation or electrode materials.[12] Numerous selective oxidation reactions have been designed to

[a]*Biorefinery Processes Group, Chemical and Environmental Engineering Department, Engineering Faculty of Gipuzkoa, University of the Basque Country UPV/EHU, Plaza Europa 1, 20018 Donostia, Spain. E-mail: jalel.labidi@ehu.eus*
[b]*University of Pau and the Adour Region, E2S UPPA, CNRS, Institute of Analytical and Physicochemical Sciences for the Environment and Materials (IPREM-UMR 5254), 403 Rue de Saint Pierre, 40004 Mont de Marsan, France*
† Electronic supplementary information (ESI) available. See DOI: https://doi.org/10.1039/d3gc01037f

cleavage and functionalize the lignin molecule, emphasizing more sustainable processes like ozonation, catalytic, photocatalytic, US irradiated, and electrochemical oxidation, where more energetically efficient processes are designed.[13] For example, Garedew *et al.* reported works where electrocatalytic oxidation processes were carried out at ambient temperature and pressures, where different products were obtained by adjusting the potential.[14] Different transition-metal complexes were used to catalyze the process,[15] or alternative solvents like protic ionic liquids[16,17] were employed. Alternatively, hydrothermal oxidation,[18] enzymatic depolymerization,[19,20] and functionalization[21,22] procedures have been carried out. The most common products obtained by these processes are the low molecular weight phenolic compounds (LMWPC), such as phenolic aldehydes, ketones, and acids.[23]

Conversely, oxidative fractionation of lignin into dicarboxylic acids (DCAs) like muconic, maleic, and succinic acids can substitute the currently used.[24] Lastly, the other family of compounds that can be obtained from the oxidation of lignin is the oxidized derivatives of aromatic compounds, also known as quinones. These molecules are interesting because they can act as catalysts in Kraft processes to enhance the performance of the pulping process and as redox-active organic molecules, plausible to replace the redox-active metals presently used in energy storage, leading to the incorporation of a biomass-derived and inexpensive material.[25]

An extended amount of work investigating lignin oxidation is based on incorporating and utilizing different chemical catalysts (homogeneous and heterogeneous). A wide variety of compounds have been used as catalyzing agents, starting from the most common metallic ones (like Cu[26]) to TiO_2 doped with bimetals like Cu–Au or Fe–Au,[27] as well as KOH[28] or KO^{t}Bu.[29] These catalytic agents have been widely used along with other oxidating agents like H_2O_2, an extensively used bleaching agent in the paper industry.[30] A weak acid dissociates into a strong nucleophile perhydroxyl anion (HOO^-), attacking electron-deficient functional groups like carbonyl groups and enabling lignin degradation into phenolic compounds.[31] It is highly susceptible to decomposition reactions, especially when high temperatures and pH are used.[30] It has been reported to be able to react with phenols on lignin, forming phenoxy radicals that later degrade to low molecular weight compounds. Nevertheless, these reactions happen when metals are added or pH is kept at similar values to the pK_a of the peroxide (11.7). Minor degradation reactions can still happen at milder conditions than explained, with primary reaction products from phenolic structures (primarily quinones) as yields.[32]

US irradiation is based on acoustic cavitation. Liquids irradiated in the correct conditions create, expand, and collapse vapor bubbles capable of inducing the formation of radicals by the cavitation effect.[33] This cavitation effect is formed by the implosion of the bubbles, which create localized high pressures and temperatures while the overall liquid maintains a controlled temperature. The US has been mainly used in biorefinery processes to enhance delignification processes, increasing extraction yields and purity. However, more recently, it has been observed that this technology can synthesize lignin nanoparticles, similar to the formation of nanocellulose and nanochitosan entities.[34] When lignin is subjected to ultrasonic forces, its molecule considerably reduces its size since the molecular bonds present in the structure are broken down by the energy applied in the form of cavitation effect.[35] Consequently, spherical nanolignins of diameters around 100 nm can be obtained and physically prevented from re-attaching themselves to avoid their reorganization in bigger molecules, as stated before by Gilca *et al.* and Mishra *et al.*[34,36]

This work aims to produce oxidized lignin nanoparticles, highly functionalized and with great surface area and potential to be incorporated in a varied application range. The designed route to obtain this objective was defined based on the oxidation of Kraft lignin in mild conditions with the combined action of an oxidating agent (H_2O_2) and ultrasonic cavitation in an innovative integrated mechanism not tested before. This procedure may therefore enhance a way for obtaining primary reaction products from the phenolic structures present in lignin without reaching the most widely explored path until the present day, which are low molecular weight redox-active compounds like quinones, widely investigated materials for diverse applications ranging from biologic applications due to their immunotoxic, cytotoxic, and carcinogenic properties,[37] to electrochemical applications in different types of batteries (redox-flow batteries,[38] and zinc[39] or sodium ion batteries[40]). Moreover, the obtention of nanosized particles, with an increased ratio of surface to volume, has improved properties, opening new possibilities for the lignin incorporation in a wider range of applications like cosmetics,[41] polymer nanocomposites with enhanced mechanical properties, or even energy storage materials.[42]

Results and discussion

Design of experiments (DOE)

Eighteen experiments were designed using a multilevel factorial method, where T, t, and [H_2O_2] were chosen as experimental factors. T and t were 3 level factors, with 30, 45, and 60 °C and 15, 30, and 60 min as level values, respectively. [H_2O_2], on the other hand, was a 2-level factor, where 0.0 and 0.1 eq. H_2O_2 to lignin was used. Estimations for each of the experimental effects and the interactions obtained are listed in Table S1,† data of variance for Z potential in Table S2,† standardized Pareto Diagram for Z potential in Fig. S1,† and Graph of main effects for Z potential are shown in Fig. S2.† The F-values shown in Table S2† show the variations between the means of the sample. The higher the value of F, the greater the difference between the group means, evidencing the difference the treatment has on the samples. The p-value, meanwhile, concludes if there is a statistically significant difference between the means of the three groups. When this value is equal to or higher than 0.05, there is evidence to conclude a statistical difference between the group means. Fig. S1† shows that H_2O_2 addition is the parameter that affects the most the Z

pot value, followed by time. Nevertheless, Fig. S2† shows that these effects are detrimental to particle stability, as Z pot values increase with H_2O_2 addition and higher *T*-s, while it decreases with longer times.

Yield, pH change, and total energy delivered to the system

The total amount of energy delivery to the system was recorded for each sample, which is related to the ultrasonic power and elapsed time by the following equation:

$$E = P \cdot t \quad (1)$$

where E is the energy delivered to the system, P is the ultrasonic power, and t is the elapsed time.

The yields obtained, shown in Fig. 1 and listed in Table S3,† are similar for most of the samples, which means that the product loss is due to the different stages of the process, such as precipitation, centrifugation, and filtration. Even though a considerable amount was lost (around 25%), optimizing the recovery stages could easily reduce this value. In terms of energy delivered to the system, visible in Fig. 1, the tendency followed was linear with time. H_2O_2 addition significantly affected the pH variation during the reaction, considerably decreasing the value due to the acidic nature of the compound and its disassociation into HOO^-. In the experiments where peroxide was not added, the pH remained almost constant; however, its addition decreased pH values. It is observable that the increase in sonication time favored the dissociation of H_2O_2 at medium and high temperatures since the pH decreased considerably more than at low temperatures.

Chemical composition and elemental analysis of the samples

Oxidized lignin samples were analyzed by QAH, UV-vis spectroscopy, HPLC, and TGA, which enabled the quantification of Acid Insoluble Lignin (AIL), Acid Soluble Lignin (ASL), carbohydrates (CA), and ash content. The mass content of the major components of the samples is illustrated in Fig. 2 (left) and listed in Table S4.† QAH effectively quantifies the purity of the lignin obtained (AIL) to estimate the degree of degradation and quantify the side products (CA, ASL, Ashes...) of each experiment. KL has the least amount of AIL, corresponding to the sample with the highest content of impurities. After oxidation, AIL content increased from 15% to almost 20%. ASL content decreases considerably, meaning many of these molecules were dissolved during the process. The CA content increased due to the degradation products obtained from the oxidation, the most noticeable rise being in the last three reactions, where hydrogen peroxide and 60 °C were used. The harsher conditions improve the dissociation of lignin into smaller molecules, such as carboxylic acids or carbohydrates. The ash content, however, decreased with the oxidation reactions. The initial Kraft lignin presented high inorganic matter, resulting in low purity. Reactions with longer times showed decreased ash content, resulting in a high-purity product.

The results obtained from the Elemental Analysis are illustrated in Fig. 2 (right), and values are listed in Table S5.† Carbon, hydrogen, nitrogen, oxygen, and sulfur content were determined, useful to deduce how external functional groups to lignin (HOO^- from the peroxide or SO_4^{2-} from the sulphuric acid used for precipitation) adhere to the samples depending on the reaction conditions. KL is primarily composed of carbon (62.44 ± 0.38%); however, carbon content increased with the sonochemical oxidation, reaching up to 66.41 ± 0.76% in the case of OxL9. The second most abundant element in lignin biopolymers is oxygen, with values around 25%. KL was the sample with the highest O content, with 26.98 ± 0.54%, while most of the oxidized lignins had around 23–24%, the least being the OxL3 with 23.41 ± 0.28%. However, this does not necessarily mean that KL is the sample with the highest functionality. Lignin macromolecules are formed by crosslinking monolignols through several linkages, ether bonds being the most common. Therefore, the high

Fig. 1 On the left side is the yield after each sonochemical treatment, and the right diagram represents the total energy delivered to the system and the change in pH during the reaction for the different oxidative conditions.

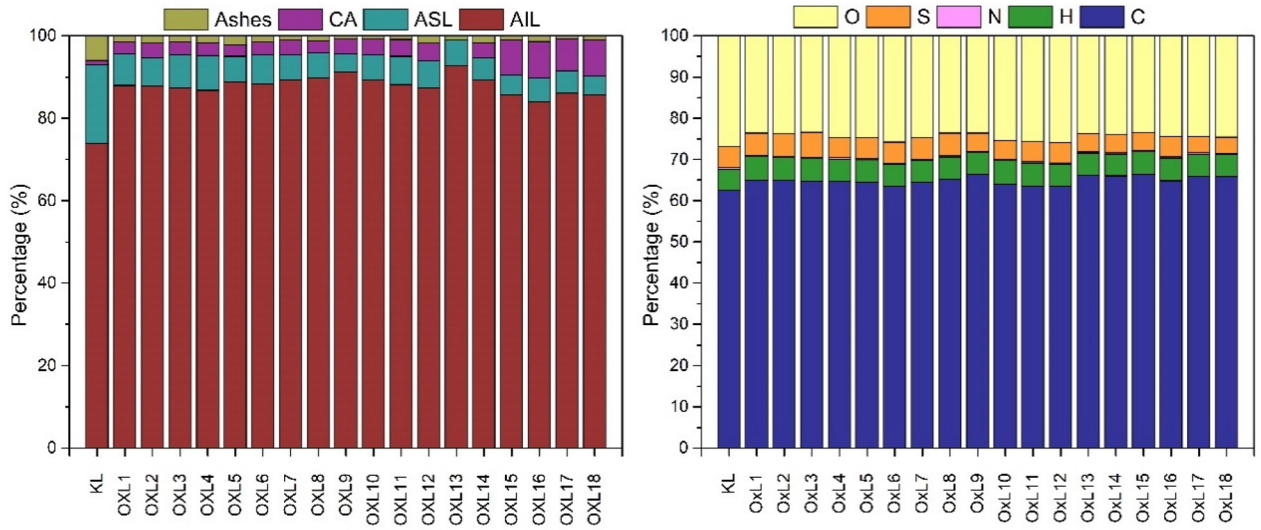

Fig. 2 Chemical composition (left) and elemental composition (right) of KL and the oxidized samples.

amount of O can be related to the high amount of ether groups rather than hydroxyl or carbonyl.[43] In terms of hydrogen, it increased with the reaction time, with the set point at 5.20 ± 0.02% and reaching values of 5.69 ± 0.19%; the same trend followed throughout the samples.

Regarding S content, KL contains 5.07 ± 0.16%, increasing to 6.08 ± 0.05% in the case of OxL3 and decreasing to 3.93 ± 0.11% in the case of OxL18. This might be influenced by the temperature in which the reaction occurred, contributing to the pH change. In the case of the lowest temperature conditions (30 °C), the lignins obtained have higher S content and lower O content than the ones compared with the samples obtained at the highest temperature conditions (60 °C). This also concurs with the pH change and, consequently, the dissociation of H_2O_2 to HOO^-. The samples obtained at 30 °C had fewer HOO^- ions to associate with, so when precipitated with H_2SO_4, they had more active sites for the adhesion of S atoms. Conversely, the samples obtained at 60 °C had a higher content of HOO^- ions, promoting their attachment before the precipitation with H_2SO_4. Finally, the N content did not fluctuate in the process, which is insignificant, to the point where it could be considered N-free. This parameter, however, is determined by the nature of the raw material rather than by the process.[44]

Table 1 Average molecular number (M_n), average molecular weight (M_w), and polydispersity index ($Đ_M$) of the different lignins

	M_n (g mol^{-1})	M_w (g mol^{-1})	$Đ_M$
KL	856	2590	3.0
OxL1	828	2497	3.0
OxL2	852	2532	3.0
OxL3	849	2595	3.1
OxL4	851	2608	3.1
OxL5	871	2690	3.1
OxL6	901	2887	3.2
OxL7	860	2583	3.0
OxL8	876	2678	3.1
OxL9	1029	3580	3.5
OxL10	964	3204	3.3
OxL11	898	2821	3.1
OxL12	930	3002	3.2
OxL13	933	3071	3.3
OxL14	1003	3549	3.5
OxL15	1005	3549	3.5
OxL16	897	2774	3.1
OxL17	933	3168	3.4
OxL18	945	3348	3.5

Physicochemical properties of the samples

The average molecular number (M_n), average molecular weight (M_w), and polydispersity index ($Đ_M$) values for KL and the oxidized samples are listed in Table 1, and the chromatogram curves obtained for each sample are shown in Fig. S3.† Overall, M_w increased slightly in the process, validating that mild oxidation conditions are not enough for the degradation and depolymerization of the lignin, maintaining the molecular structure relatively stable. It can be observed that values stayed similar to the original sample (KL) or increased slightly. The increase in the values could be attributed to condensation reactions happening after the creation of radicals and their following association. Moreover, this condensation phenomenon happened when the reaction conditions were aggravated, especially time and temperature. When the temperatures used were low (30 °C), time did not affect the M_w (M_w(OxL1) ≈ M_w(OxL2) ≈ M_w(OxL3)). However, when T increased to 45 °C, the M_w increased slightly and significantly when t-s increased to 30 and 60 min, respectively (M_w(OxL7) < M_w(OxL8) ≪ M_w(OxL9)). Adding H_2O_2 also promoted a slight increment in M_w, although this change was not remarkable. Finally, it was observed that with high T (60 °C), time did not influence between 30 and 60 min, nor with the addition of H_2O_2 (M_w(OxL17) ≈ M_w(OxL18)), nor without H_2O_2 (M_w(OxL14) ≈ M_w(OxL15)). This phenomenon can be observed from the

curves obtained, since samples OxL9, OxL13, OxL14, and OxL15 are the ones from which the most significant change can be observed, with the highest peak at a retention time of around 21 min, signifying a higher M_w proportion.

In terms of polydispersity, the changes were not substantial. A similar phenomenon attributed to the change in M_w could be applied, where mild conditions in the reaction did not affect the molecular composition. In contrast, the higher conditions created new molecular structures due to bond cleavages and recondensation, increasing the general heterogeneity. Still, the increase in $Đ_M$ can be considered neglectable.

The FTIR spectra are illustrated in Fig. S4,† and the assignments for each frequency range are listed in Table S6.† Structural features and functional groups of the lignins can be observed. The broad bands obtained at 3400 cm^{-1} are attributed to O–H stretching in aliphatic and phenolic hydroxyl groups. This band intensified in all the oxidized samples, meaning the OH content increased during the process. C=O stretching, attributed to bands at 1708 cm^{-1}, also increased, more clearly seen in a close-up look in Fig. S5.†

On the other hand, aromatic skeletal vibration bands at 1610 cm^{-1} slightly decreased their intensity with the oxidation reactions, along with the bands at 1329 cm^{-1} and 1217 cm^{-1}, attributed to S ring and G ring stretching. This means that a mild decomposition happened in lignin due to aromatic cleavage. Moreover, the decrease in intensity of the bands at 1150 cm^{-1} implies a decrease in aliphatic ether groups. Consequently, aromatic rings and aliphatic ether bonds cleaved increased carboxylic and hydroxyl groups, especially for samples reacted for extended times and low temperatures (30 °C, OxL3) and medium times for medium temperatures (45 °C, OxL8, and OxL11), either with or without the addition of hydrogen peroxide. At high temperatures (60 °C), the lack of H_2O_2 favored the process, and short and long periods were the ones exhibiting the most differences (OxL13 and OxL15).[45]

The amount of OH mmol quantified by the Folin–Ciocalteu method is illustrated in Fig. S6.† Overall, the total phenolic content decreased. As seen from the FTIR, aromatic rings suffered cleavage, causing degradation of the phenolic compounds of lignin and forming quinones.[46] The more the TPC decreases, the harsher the oxidation conditions and the more degradation occur. Since these conditions are kept mild, and the QAH analysis corroborates that a considerably low amount of CA is obtained, it is evident that although lignin reacts, the reactions finish before high degradation of lignin occurs, ensuring the preservation of its integrity throughout the process. The fluctuation in the TPC did not follow any linearity with the increase in time.

In some cases, shorter times favored the increment of TPC, while in other times, specifically when temperatures were also higher, longer times led to molecules with more OH groups. At short times (15 min), the temperature increase aggravated its loss, showing a linear trend (a decrease from 0.013 mmol g^{-1} at 30 °C, to 0.095 mmol g^{-1} at 45 °C, to 0.009 mmol g^{-1} at 60 °C). When H_2O_2 was added, the trend followed was similar; OH concentration decreased inversely proportionally with time. Medium times were the optimum at medium temperatures, while long times had the best results at high temperatures.

This could be because low temperatures do not allow breaking aromatic rings, and substituting aliphatic and phenolic OH groups does not require extended time. On the other hand, because the increase in temperature aggravates the reaction conditions, short times are sufficient for partial lignin aromatic ring cleavage, and new functional groups like hydroxyl groups are created. However, longer times tend to repolymerize, again decreasing the OH content, as condensation reactions happen in this functional group. UV absorption bands were also recorded from 400 to 260 nm, illustrated in Fig. S6.† The absorption peaks at 280 nm correspond to non-conjugated OH groups, while values at 315 nm correspond to the conjugated OH groups. Samples obtained at low temperatures follow the same trend as in TPC, where longer times reduce the OH content the most, both conjugated and non-conjugated. All samples reduced their content in conjugated and non-conjugated OH groups, although this change was irrelevant. Nevertheless, medium temperatures were the ones that reduced the quantity of these functional groups most, while high temperatures were the ones that reduced the least and the most similar, albeit changing time and adding H_2O_2.

Different OH groups in lignin were identified and quantitatively determined by ^{31}P NMR spectroscopy. Peaks associated with aliphatic OH, C5-substituted OH, guaiacyl OH, *p*-hydroxyphenyl OH, and carboxylic acid OH were integrated and compared with the integration value obtained for the internal standard (NHND) to get mmol g^{-1} lignin concentration values. Besides, S/G ratios were also obtained. The results are listed in Table 2, and the spectra are represented in Fig. S7.† All samples lacked from H unit due to the hardwood origin of the Kraft lignin; overall, an increase in OH content can be observed for all the treated samples. The increase in hydroxyl content indicates that the conditions used are not strong enough for condensation or depolymerization reactions, which validates these conditions as suitable for the oxidation of lignin. Ultrasonic forces fragment the condensed structures. Therefore, S and G units free themselves from the macromolecule, regaining the OH group from which condensation occurred. Since the C5 of the aromatic ring is free in G units, their reactivity is higher and easier to condense. Consequently, G units are more abundant in condensed structures, and when fractioned, the released units are also G units.[47]

Total phenolic hydroxyl content increased in all treated samples. The lowest temperatures without adding hydrogen peroxide were even more efficient for an increment in phenolic OH content (OxL1 and OxL2), where the most extended times were most effective (OxL3). OxL3 obtained the optimal results, with the highest OH content, both aliphatic and phenolic. This differs from the results obtained from the Folin–Ciocalteu method, where longer times led to less TPC at the lowest *T*.

The efficiency in medium and high temperatures, with the addition of H_2O_2, was not so satisfactory, meaning the harsher

Table 2 Quantification of different hydroxyl content (mmol g^{-1} lignin) and S/G ratio for selected samples

	Aliphatic OH	C5-substituted (S) OH	Guaiacyl (G) OH	*p*-Hydroxyphenyl (H) OH	Carboxylic acid OH	Total phenolic OH	S/G ratio
KL	0.05	0.18	0.06	—	0.04	0.24	3.17
OxL1	0.06	0.21	0.07	—	0.03	0.28	2.86
OxL2	0.06	0.20	0.07	—	0.03	0.27	2.86
OxL3	0.07	0.25	0.09	—	0.03	0.34	2.89
OxL9	0.06	0.20	0.06	—	0.04	0.26	3.08
OxL16	0.06	0.20	0.07	—	0.03	0.27	2.83
OxL17	0.06	0.21	0.07	—	0.04	0.28	2.88
OxL18	0.04	0.20	0.07	—	0.01	0.27	2.67

conditions did not positively influence the results (OxL9 and OxL18). Low and medium times, nevertheless, showed better results in the harshest conditions (OxL16 and OxL17) than longer times (OxL18). However, once again, these results are not in concordance with the ones obtained with those obtained with the Folin method since the TPC measured had medium values with sample OxL9, and an increase could be observed with the increment with time when the harshest conditions were applied (60 °C and H_2O_2).

Aliphatic OH groups also increased in all samples except for OxL18, which decreased due to condensation. Aliphatic hydroxyl groups are more reactive than phenolic hydroxyl groups,[47] meaning that these conditions might be where condensation reactions start instead of oxidation. In carboxylic acid OH groups, a clear tendency could not be observed; although medium conditions like low temperature and medium time (OxL2) and high temperature and low time (OxL16) obtained less COOH content, harsher conditions favored the appearance of more groups. Nevertheless, OxL18 was the sample with the considerably lowest COOH content, following the same mechanism that caused the reduction of the aliphatic content.

In terms of the S/G ratio, all treated samples reduced their S/G ratio, meaning that the quantity of G units increased more than S units. OxL18 was the one that obtained the smallest ratio, but observing the individual concentrations of G and S OH, OxL3 was the most effective in increasing both S and G units, considerably increasing the value of S OH mmol, the hardest compound to react, while using low temperatures with no addition of oxidizing agent. This matches with the results obtained in FTIR spectra, where the band intensity at 1150 cm^{-1} decreased, presuming the cleavage of aliphatic ether bonds and increasing C=O and OH groups. This happened at low temperatures and without the addition of hydrogen peroxide because ultrasound irradiation is efficient at low temperatures, enabling the oxidation of lignin without further undesired phenomena like agglomeration, depolymerization, and degradation. The quantity of oxidized functional groups increased with the prolongation of the reaction time, whereas the conditions were too mild for the occurrence of further reactions. When heat and H_2O_2 are supplied, these other reactions start, exceeding the oxidation step intended and leading to obtaining degraded samples.

Thermal properties of the samples

Thermogravimetric Analysis (TGA) was performed for each sample. The obtained TGA and DTGA curves are illustrated in Fig. S8,† and the values of mass loss at 5% and 50% ($T_{5\%}$ and $T_{50\%}$) along the degradation stages are listed in Table S7.† $T_{5\%}$ corresponds to the temperature at which 5% of the mass degrades. Overall, most samples have a $T_{5\%}$ between 150 and 200 °C. Typically, moisture is evaporated before, meaning its content is lower than 5%, except for OxL5 and OxL6, where their $T_{5\%}$ is at 75 °C. $T_{50\%}$ corresponds to the temperature in which 50% of the mass is lost. Most $T_{50\%}$ values are around 425 and 475 °C, with few exceptions exceeding that (OxL4 with 540 °C and OxL15 with 520 °C).

DTGA curves depict the different degradation stages happening at different temperatures. The first degradation stages happening below 150 °C are due to moisture loss. The second degradation stage happens between 200 and 300 °C, corresponding to the degradation of polysaccharides and aliphatic alcohols and acids. Finally, aromatic ring cleavage and degradation of syringyl and guaiacyl units into phenolic compounds happen at temperatures above 300 °C.[48,49]

The first degradation step is due to the moisture loss of the sample, happening at 50–60 °C in all cases. The second significant mass loss happened around 200 and 300 °C, with minor degradation. In this step, small molecules were degraded, while the main part of the lignin sample was lost between 350 and 460 °C. Finally, a few samples had residual matter, which degraded at around 700 °C. OxL4 and OxL15 have the highest thermal stability, while OxL1, OxL8, and OxL16 have the lowest. This might be due to the condensed structures being more considerable in the first ones and scarcer in the last ones. The main degradation temperatures were also higher for samples OxL4 and OxL15, while KL and OxL5 had the lowest.

Differential Scanning Calorimetry (DSC) curves can be seen in Fig. S9,† and the T_g-s obtained are listed in Table S7.† It can be observed that values ranged around 116–118 °C or around 97 °C. This fluctuation of T_g values can be related to the heterogeneous nature of lignin samples since a correlation between T_g and $Đ_M$ was noticed. KL and other oxidized samples maintained a similar polydispersity value, around 3.0–3.3, while samples OxL9, OxL14, OxL15, OxL17, and OxL18 have a $Đ_M$ value of 3.4–3.5. This small increase in $Đ_M$ entailed a reduction of the T_g of almost 20 °C, detrimental to the rigidity when temperatures reach that T_g value.

Morphological properties of the samples

Z potential (mV), conductivity (mS cm^{-1}), size average (nm), and dispersity index were measured for all samples by Diffraction Light Scattering (DLS). The Z potential (ZP) refers to the value of the electric charge of the surface of the particle, which can determine the stability and the tendency of the particles to aggregate themselves. High ZP values (positive or negative) imply that they have good physical stability due to the electric repulsion and the high charge surface, disabling the aggregation and growth in size. Values between +30 mV and −30 mV indicate instability, with van der Waals forces being able to act upon the particles, creating aggregates. When this value is higher than +30 mV or minor than −30 mV, the particles have sufficient repulsive force to be physically stable in dispersion. From Fig. 3, most lignins presented moderate stability, while some presented incipient stability. KL has incipient stability; however, most samples have values from −30 mV to −40 mV. This means that the process was effective in forming more stable particles. Three samples reached really good stability, OxL1, OxL2, and OxL3. These were obtained at the lowest temperature (30 °C), at various times, without adding H_2O_2. It was observed that ZP decreased with sonication time almost linearly, a trend that was similar in samples obtained at 45 °C (OxL7, OxL8, and OxL9), and 60 °C (OxL13, OxL14, and OxL15), without H_2O_2. These higher temperatures, nevertheless, created more unstable particles. The reason might be that these stronger conditions promote lignin degradation into smaller particles and repolymerization, which are less stable particles with a higher dispersity index. Particle size was measured similarly. Values are obtained by the photon dispersion fomented by the particle dispersed in water, which depending on the particle size and how this interacts with the medium, disperses differently and obtains different values. It is an interesting method to give a quantitative value of the particle size due to the rapid measurement and easy obtention of the data. However, the information obtained might differ from other qualitative methods like SEM o TEM since these particles observed are no longer dispersed or dissolved when analyzed.

There was not a visible correlation between ZP and size average. Nevertheless, the smallest particles, OxL3 and OxL18, had the highest conductivity values, almost doubling the values of the other samples. These two samples had the longest reaction times, contributing to higher H content, probably due to the formation of hydroxyl groups that improve

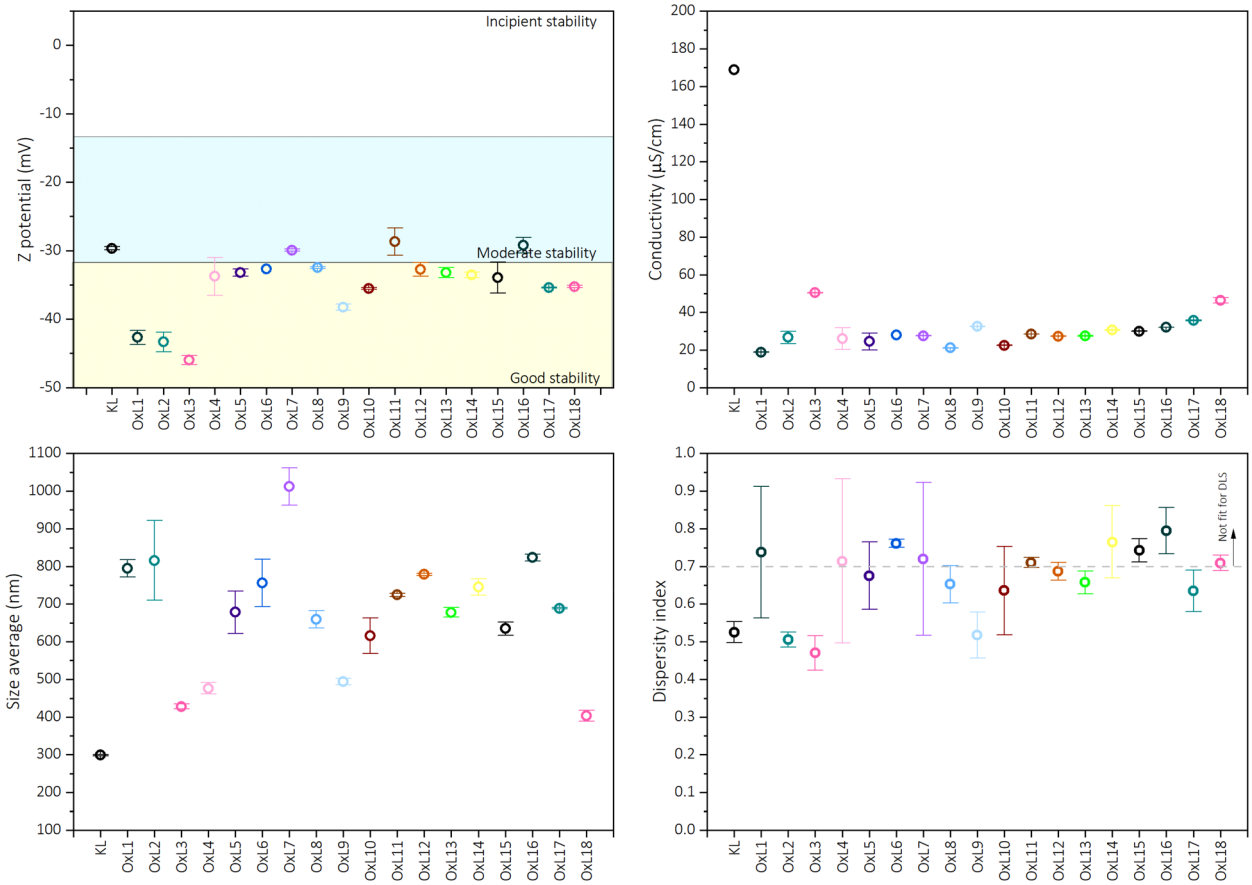

Fig. 3 Stability of lignin particles. Z potential (mV), conductivity (mS cm^{-1}), size average (nm), and dispersity index (from left to right and top to bottom).

stability. Overall, regarding morphological properties, OxL3 is the sample with the best results since it has the highest ZP, highest conductivity, smallest size, and lowest dispersity index.

Selected lignin particles were dispersed in water at a concentration of 0.1 wt% and prepared for TEM analysis. The images obtained at a 500 nm scale and negative contrast are shown in Fig. 4, and aggregate particle types and average particle size values are listed in Table S8.† It should be mentioned that the size values obtained from DLS and TEM differ due to the nature of the analyses. The first is measured by dispersing samples in a liquid media and measuring the light scattering of dispersed bodies, while the latter is dried and just particles are imaged. Therefore, size values obtained from DLS are higher, but a similar trend in the values change can be observed from both.

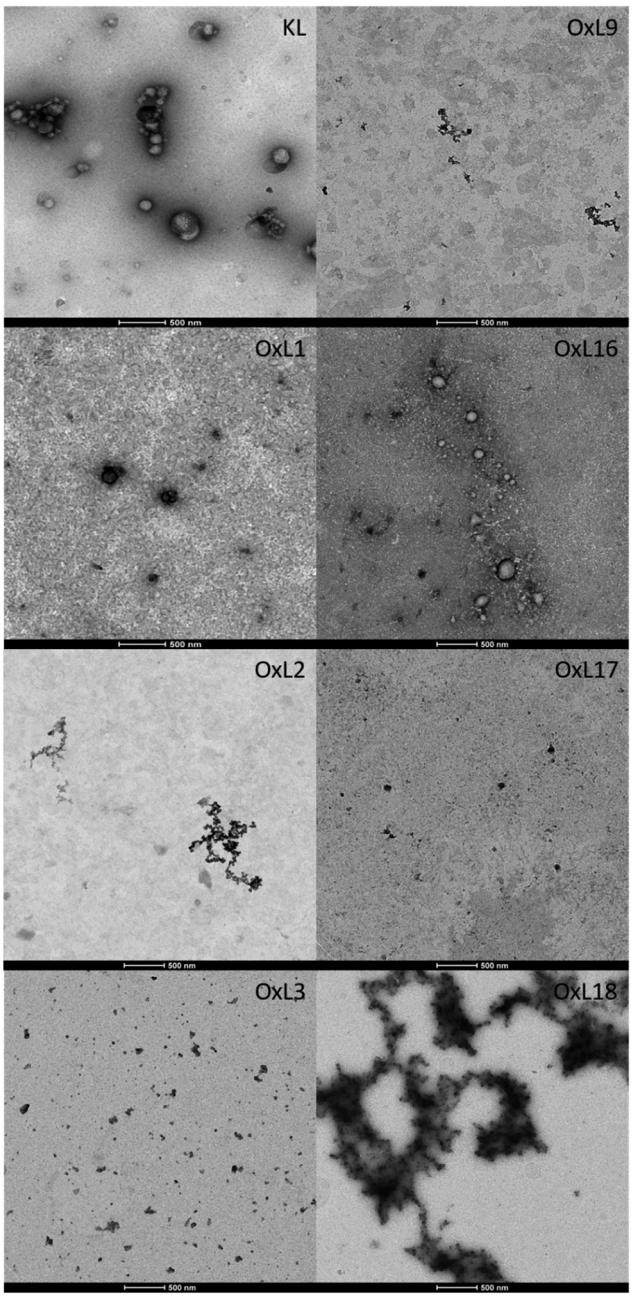

Fig. 4 TEM images of KL, OxL1, OxL2, OxL3, OxL9, OxL16, OxL17, and OxL18.

Images obtained by TEM display that the reaction reduced the sizes and influenced the dispersion, aggregation, and agglomeration of the lignin particles. KL particles had considerably bigger diameters than the sonochemically oxidized samples, which demonstrated the influence of the process on the final particles when times were medium or high. The average particle size of OxL1 and OxL16 maintained quite similar to the value of KL, obtaining particles with diameters ranging from 125–150 nm, regardless addition of H_2O_2 and T. With the increase of t at low temperatures (OxL2 and OxL3), a drastic reduction of size could be observed, where 25 nm sized particles were measured. A decrease was also observed with time in the case of OxL17 and OxL18, but the particles obtained did not reduce so drastically. Medium T and long t were also effective for the obtention of nanolignin (OxL9) since the smallest particles quantified by this technique were these. Another interesting parameter observable by this technique is the variability of the tendency to create particle clusters. KL particles were tightly bound, creating agglomerations. These clusters reduced significantly even with the mildest reaction conditions (30 °C during 15 min), as can be observed in the image of OxL1, where the particle size is much smaller, and the agglomerates are minor. When the reaction time increased to 30 min (sample OxL2), particles switched from being tightly bound to slightly bound, creating agglomerations instead of aggregates.[50] This means that the interactions with the highest force were broken and substituted by others with lighter force. When time increased to 60 min, particle–particle forces were hardly noticeable, mostly finding free particles (OxL3). Agglomerations reoccurred when the temperature increased to 45 °C while maintaining the longest time (OxL9). This phenomenon magnified significantly when the temperature increased to 60 °C while maintaining the one-hour reaction time (OxL18). It can be concluded that reaction time influences more the agglomeration formation than the reaction temperature, as the samples obtained at 60 °C after 15 and 30 min (OxL16 and OxL17, respectively) were loose molecules with no visible particle–particle interactions. Moreover, the addition of H_2O_2 has no apparent effect on it either. It has also been established that the particles with higher molecular weights have smaller particle sizes[51] since they initiate the nucleation in the lignin precipitation and have a more hydrophobic nature. The lack of small M_w lignins means that they will not coat the larger molecules, as they are the ones that precipitate subsequently.[52]

Scaling up perspectives

The use of ultrasound irradiation has been widely evaluated for pilot and industrial scales, where both technical and economic feasibilities have been studied. The energy density (E_s) is a key factor for determining this since it takes into account the main parameters of the sonication treatment: power, duration,

and volume.[53] However, the processing type should be similar to have a solid scaling.

The current work experiments were carried out at three different times (15, 30, and 60 min). Other conditions like T and $[H_2O_2]$ did not considerably affect the E_s of each experiment, as seen in Fig. 1. Experiments with 15 min of duration consumed overall around 50 kJ, while the ones with 30 and 60 min consumed around 75 and 250 kJ, respectively. The volume of the solutions prepared and sonicated was 60 mL for all of them. Therefore, 800, 1250, and 4170 kJ L^{-1} were consumed for 15, 30, and 60 min treatments.

In terms of overall sustainability, there have been works where certain metrics have been applied to consider processes as green.[4] Generally speaking, the proposed process complies with this category, due to the utilization of waste derived from the paper and pulp industry, with no conflicting interests with alimentary products, and with the implementation of ultrasonic cavitations. Moreover, this work has concluded that adding peroxide as an oxidating agent has detrimental effects, and no other catalyst compounds have been added, easing the posterior processing of the obtained waste or side products of the designed process.

Experimental

Materials

Kraft liquor was kindly supplied by a local paper mill (Zikuñaga, Hernani, Spain). Concentrated H_2SO_4 (7664-93-9, 96% technical grade, PanReac) was used to precipitate Kraft lignin (KL). NaOH (1310-73-2, for Analysis, CS, ISO, PanReac) and H_2O_2 (7722-84-1, 50%, Sigma-Aldrich) were used for the oxidation reaction. *N*,*N*-Dimethylformamide (DMF, 68-12-2, 99.5%, HPLC grade, Fisher), and LiBr (7550-35-8, PanReac) were used for the GPC. Dimethyl sulfoxide (DMSO, 67-68-5, ACS, PanReac), Na_2CO_3 (497-19-8, 99.8%, Scharlab), Folin–Ciocalteu reagent (12111-13-6, Scharlau), and gallic acid monohydrate (5995-86-8, Sharlau) were used for the total phenolic content determination. 1,2-Dioxane (123-91-1, ≥99.8%, Alfa Aesar) was used to determine conjugated and non-conjugated OH groups. Pyridine (Py, 613-002-00-7, anhydrous, 99.8%, Sigma-Aldrich), deuterated chloroform ($CDCl_3$, 865-49-6, "100%", 99.96 atom % D, Aldrich), chromium(III) acetylacetonate ($Cr(acac)_3$, 21679-31-2, 97%, Aldrich), *endo*-*N*-hydroxy-5-norbornene-2,3-dicarboximide (NHND, 21715-90-2, 97%, Aldrich) and 2-chloro-4,4,5,5-tetramethyl-1,3.2-dioxaphospholane (TMDP, 14812-59-0, 95%, Sigma-Aldrich) were used for the ^{31}P NMR.

Sonochemical oxidation of lignin

Oxidized lignin nanoparticles were synthesized using different conditions and combined accordingly by an experimental model designed by STRATIGRAPHIC Centurion XV. A Factorial Multilevel design was chosen, with three experimental factors with different levels (3 levels for T and t and two levels for $[H_2O_2]$) and one response variable (Z potential). Eighteen different experiments were designed, and the precise conditions for synthesizing each sample are presented in Table 3. Briefly, Kraft lignin was dissolved in a 1 : 20 (w/v) proportion of NaOH 4% (wt%) at room temperature (RT) for 2 h with magnetic stirring (400 rpm). Then, H_2O_2 (50%) was added in a 0.1-equivalent ratio with lignin for selected samples. The temperature was set to 30 °C, 45 °C, and 60 °C, and reactions were carried out for 15, 30, and 45 minutes. The selected operation conditions (low temperature and reaction time) with the intensification provided by the sonication allow for similar results to those reported in the literature.[34,54] The reactions were performed inside a 100 mL jacketed cell using a 20 kHz VCX 750 power supply (Sonics & Materials, USA) equipped with a piezoelectric converter connected to a 13 mm titanium alloy horn (Ti-6Al-4V) with the amplitude set at 57.5 μm; the temperature was kept stable with the help of a high precision thermostat (Huber, Germany) connected to the processing cell. Once the reaction was finished, the product was precipitated using two volumes of sulphuric acid solution (2%). Next, the precipitate was centrifuged and washed three times. Finally, the washed lignins were filtered under pressure with a filter holder (Sartorius, Germany) equipped with a nylon filtering membrane of 0.22 μm pore size and dried at 30 °C.

Determination of structural carbohydrates and lignin

Quantitative acid hydrolysis (QAH) was performed to determine the purity of the oxidized lignin samples.[55] A quantity of 0.25 g of sample was dissolved in 2.5 mL of H_2SO_4 72% (v/v) at 30 °C for 1 h. Afterward, they were diluted with H_2SO_4 2.5% (v/v) and autoclaved at 121 °C for 1 h. Finally, the solubilized lignin was separated by filtration from the remaining insolubilized solid (known as Acid Insoluble Lignin (AIL) or Klason lignin). Klason lignin was determined by gravimetric Analysis, and the soluble lignin, dissolved in the liquor, was diluted using H_2SO_4 1 M and measured its absorbance at 205 nm. HPLC also was used to quantify the carbohydrates present in

Table 3 Reaction conditions for sonochemical oxidation of lignin

Sample	$[H_2O_2]$ (eq)	T (°C)	t (min)
KL	—	—	—
OxL1	0	30	15
OxL2	0	30	30
OxL3	0	30	60
OxL4	0.1	30	15
OxL5	0.1	30	30
OxL6	0.1	30	60
OxL7	0	45	15
OxL8	0	45	30
OxL9	0	45	60
OxL10	0.1	45	15
OxL11	0.1	45	30
OxL12	0.1	45	60
OxL13	0	60	15
OxL14	0	60	30
OxL15	0	60	60
OxL16	0.1	60	15
OxL17	0.1	60	30
OxL18	0.1	60	60

the liquor. A Jasco LC Net II/ADC chromatograph with a refractive index detector was used to identify specific monomers, such as glucose, xylose, arabinose, galacturonic acid, acetic acid, furfural, and hydroxymethylfurfural. For this, 20 μL of the liquor was injected and eluded with 0.005 M H_2SO_4 at a 0.6 mL min^{-1} flow rate. The column used was an Aminex HPX-87H 300 × 7.8 mm (Bio-Rad Laboratories, USA) at 50 °C. All samples were analyzed in triplicate.

Elemental analysis (EA)

The elemental analyzer equipment used was Leco TruSpec Micro. An amount of 2 mg of sample was heated at 1050 °C, and pure helium (3× Nippon Gas) and extra pure oxygen (4× Nippon Gas) was used as carrier gas and test gas, respectively. The samples were analyzed in triplicate, and sulfamethazine Leco (C = 51.78%; H = 5.07%; S = 11.52%; O = 11.5%; N = 20.13%) was used for the calibration.[56]

Physicochemical analysis

Molecular weight (M_w), molecular number (M_n), and molar-mass dispersity (D_M) of Kraft lignin and oxidized lignins were determined by Gel Permeation Chromatography (GPC). The device used was an LC-Net II/ADC equipped with a RI-2031 Plus Intelligent refractive index detector (Jasco, Japan), PolarGel-M column (300 mm 7.5 mm), and PolarGel-Mguard (50 mm 7.5 mm). The operation was performed at 40 °C with DMF and 0.1% of LiBr as the elution solvent at a 0.7 mL min^{-1} flow rate. Lignin samples were prepared to a 5% (m/v) concentration using the same mobile phase; 20 μL of each was injected into the device. Polystyrene of various molecular weights was used as a standard for calibration.[57] The solutions were fully solubilized, but a 0.45 μm syringe filter was used to avoid any contamination entering the column.

Fourier-transformed Infrared (FTIR) spectra were recorded in FT/IR-4700 Spectrometer (Jasco). The wavenumber range was defined from 4000 to 400 cm^{-1}, with a resolution of 4 cm^{-1} and 64 scans.[58]

The spectrophotometric method of Folin–Ciocalteu was used to determine the total phenolic content (TPC) of the oxidized lignins. Solutions were prepared as followed: 0.5 mL of 2 g L^{-1} of lignin dissolved in DMSO, 5 mL of Folin–Ciocalteu reagent, and 2.5 mL of 200 g L^{-1} of Na_2CO_3 dissolved in water were added in 50 mL flasks and filled with distilled water until the indicated volume. Flasks were covered to avoid undesired reactions with light and immersed in a water bath at 40 °C for 30 minutes. Absorbance values were recorded at 715 nm of wavelengths right after the reaction in a V-730 spectrophotometer (Jasco). The same procedure was followed for the calibration curve measurements, where gallic acid solutions ranging from 1000 to 100 mg L^{-1} were prepared and used in the solutions with the Folin–Ciocalteu reagent. Absorbance values were recorded, and a calibration curve was calculated.[59]

The UV-vis spectrophotometer was also used to determine the conjugated and non-conjugated OH groups of the samples. ≈5 mg of the lignin sample was dissolved in 10 mL of dioxane : H_2O (95 : 5 v/v%). Once the sample was completely solubilized, 1 mL of the solution was diluted in 9 mL of dioxane : H_2O (50 : 50 v/v%), and the absorbance bands of these last sample solutions were recorded between 400 nm and 260 nm.[60]

^{31}P NMR was used to quantitatively determine the hydroxyl groups and the S/G ratio. Py and $CDCl_3$ were used as a solvent in a ratio of 1.6 : 1 (v/v), both for the internal standard (IS) and sample solutions. The IS solution was prepared, adding 5 mg of $Cr(acac)_3$ and 18 mg of NHND per 1 mL. 0.1 mL of this IS solution was added to the sample solution prepared by solubilizing 50 mg of lignin in 0.5 mL of the solvent mixture. Once the samples were dissolved, 0.1 mL of TMDP was added for the phosphitylation reaction.[61] ^{31}P NMR spectra were recorded in a Bruker AVANCE 500 MHz, and MestReNova 11.0 was used for the data processing.

The OH group concentrations were quantified by comparing the integrated areas of the samples with that of the IS. Each area corresponds to different OH groups, enabling their quantification individually. For example, 144–137 ppm spectral region corresponds to the total phenolic OH content (from 144 to 141.5 ppm are C5-substituted OH groups, considered equivalent to S unit OH groups, from 140.5 to 139 ppm are G unit OH groups, and from 139 to 137 ppm are H unit OH groups), 150–145 ppm range corresponds to aliphatic OH groups and 136–134 ppm to carboxylic acid OH groups.[61]

Thermal analysis

Thermogravimetric Analysis was performed in a Q500 (TA Instruments) thermogravimeter. For each test, 10 ± 0.5 mg of lignin was put inside a platinum crucible and was heated from laboratory temperature to 800 °C with a heating ramp of 10 °C min^{-1} under a nitrogen atmosphere (40 mL min^{-1}).

Calorimetric properties of lignins were obtained with a Q20 (TA Instruments) calorimeter. For each test, 5 ± 0.5 mg of lignin was put inside aluminum hermetic pans, and water was removed by heating samples up to 105 °C until the weight was stable; the starting temperature was set at −50 °C. Heat flows of lignins were recorded from −50 °C to 200 °C with a ramp of 10 °C min^{-1} under a nitrogen atmosphere (50 mL min^{-1}).[49]

Morphological analysis

The size and Z potential of KL and the oxidized lignin particles were determined by Dynamic Light Scattering (DLS). A ZetaSizer Ultra (Malvern Panalytical) equipped with a He–Ne laser source (= 633 nm) and a scattering angle of 173° was used. Particles were dispersed in deionized water at a concentration of 0.1 wt% and immersed for 15 min in an ultrasound bath. The dispersions were measured at room temperature, and an average of 20 collections were recorded for each result.[44]

Electron microscopy was done with a TECNAI G2 20 TWIN operated at 200 kV and equipped with LaB_6 filament. Samples were prepared by first preparing a 0.1 wt% aqueous suspension, a drop of which was then suspended onto a TEM copper grid (300 Mesh) covered by a pure carbon film for 1 min. The grid was afterward blotted with filter paper and placed onto a

drop of 2% uranyl acetate for 20 seconds. It was finally washed twice using distilled water for 20 seconds each time.[62] Particle sizes were calculated using the software Image J, and ten particles of each sample were calculated to get the average particle size values.

Conclusions

Sonochemically assisted oxidation reactions of lignin were investigated by applying mild conditions, where temperature and time increment, and adding H_2O_2 as a catalyzer to obtain more functionalized lignin particles, enabling the downstream valorization process. All samples obtained were physicochemically modified. Ultrasound irradiation was efficient for obtaining lignin nanoparticles even under mild conditions, enhancing the effects of the reaction conditions. In contrast, OH groups did not increase massively in the resulting lignin samples. However, it could be observed from ^{31}P NMR technique that phenolic hydroxyl groups increase, especially at low temperatures (30 °C), with no oxidizing agent, and long times (60 min), which correspond to the OxL3 sample. FTIR spectra concluded that carboxylic groups also increased, confirming the oxidation reactions with this novel approach. Long reaction times favored oxidation reactions when temperatures were low, while medium temperatures performed better when times were also medium and not the extreme of the selected range. On the other hand, high temperatures oxidized the samples to higher degrees regardless of reaction time. Concerning morphology, OxL3 was also the sample having the highest Z potential, conductivity, and smallest size and dispersity. It can be established that, even though the concentration of the oxidized functional groups did not increase vastly, an increment of phenolic hydroxyl groups and carboxylic groups happened, validating the oxidation reactions. Beyond these chemical conversions, significant changes in morphology were observed, concluding that sonication enabled the transformation of these to further added-value applications, being a successful and sustainable option to substitute the currently used thermochemical processes.

Author contributions

N. I. data curation, formal analysis, investigation, methodology, visualization, writing – original draft. J. F. R. conceptualization, methodology, supervision, writing – review & editing. E. R. conceptualization, data curation, formal analysis, investigation, methodology, supervision, writing – review & editing. J. L. funding acquisition, resources, supervision, validation.

Conflicts of interest

There are no conflicts to declare.

Acknowledgements

The authors would like to acknowledge the Basque Government for the financial support of this research through project IT1498-22 and grant PIF19-183. E. R. wants to acknowledge the tenure track position "BOIS" part of E2S UPPA supported by the "Investissements d'Avenir" French program managed by ANR (ANR-16-IDEX-0002). The authors thank for the technical and human support provided by SGIker (UPV/EHU/ERDF, EU).

References

1 P. Manzanares, *Acta Innov.*, 2020, 47–56.
2 J. Wenger, V. Haas and T. Stern, *Curr. For. Rep.*, 2020, **6**, 294–308.
3 A. M. Da Costa Lopes, *Acta Innov.*, 2021, **40**, 64–78.
4 S. Gillet, M. Aguedo, L. Petitjean, A. R. C. Morais, A. M. Da Costa Lopes, R. M. Łukasik and P. T. Anastas, *Green Chem.*, 2017, **19**, 4200–4233.
5 K. V. Sarkanen and C. H. Ludwig, *Lignins: Occurrence, formation, structure and reactions*, 1972, vol. 10.
6 I. S. Goldstein, *Organic Chemicals from Biomass*, 1st edn, 1981.
7 Q. Xiang and Y. Y. Lee, *Appl. Biochem. Biotechnol., Part A*, 2001, **91–93**, 71–80.
8 R. Ma, M. Guo and X. Zhang, *Catal. Today*, 2018, **302**, 50–60.
9 D. E. García, N. Delgado, F. L. Aranda, M. A. Toledo, G. Cabrera-Barjas, E. M. Sintjago, D. Escobar-Avello and S. Paczkowski, *Ind. Crops Prod.*, 2018, **123**, 154–163.
10 C. Scarica, R. Suriano, M. Levi, S. Turri and G. Griffini, *ACS Sustainable Chem. Eng.*, 2018, **6**, 3392–3401.
11 H. Bian, L. Jiao, R. Wang, X. Wang, W. Zhu and H. Dai, *Eur. Polym. J.*, 2018, **107**, 267–274.
12 D. Wang, S. H. Lee, J. Kim and C. B. Park, *ChemSusChem*, 2020, **13**, 2807–2827.
13 D. Peramune, D. C. Manatunga, R. S. Dassanayake, V. Premalal, R. N. Liyanage, C. Gunathilake and N. Abidi, *Environ. Res.*, 2022, **215**, 114242.
14 M. Garedew, F. Lin, B. Song, T. M. DeWinter, J. E. Jackson, C. M. Saffron, C. H. Lam and P. T. Anastas, *ChemSusChem*, 2020, **13**, 4214–4237.
15 B. Xie, Y. Tobimatsu, K. Narita, S. Yokohata, H. Kamitakahara and T. Takano, *ACS Sustainable Chem. Eng.*, 2022, **10**, 16701–16708.
16 Z. Han, H. Jiang, A. Xue, G. Ni, Y. Sun, Y. Tang, P. Wan and Y. Chen, *J. Electroanal. Chem.*, 2022, **923**, 116814.
17 W. Ma, G. Liu, Q. Wang, J. Liu, X. Yuan, J. Xin, S. Wang and H. He, *J. Mol. Liq.*, 2022, **367**, 120407.
18 X. Zeng, G. Yin, Y. Zhou and J. Zhao, *Energies*, 2022, **15**, 8039.
19 S. Khan, K. K. Puss, T. Lukk, M. Loog, T. Kikas and S. Salmar, *Energies*, 2023, **16**, 1–13.

20 Z. Zhou, D. Ouyang, D. Liu and X. Zhao, *Bioresour. Technol.*, 2023, **367**, 128208.
21 S. González-Rodríguez, T. A. Lu-Chau, X. Chen, G. Eibes, A. Pizzi, G. Feijoo and M. T. Moreira, *Ind. Crops Prod.*, 2022, **186**, 115253.
22 A. G. Morena, A. Bassegoda, M. Natan, G. Jacobi, E. Banin and T. Tzanov, *ACS Appl. Mater. Interfaces*, 2022, **14**, 37270–37279.
23 W. Schutyser, T. Renders, S. Van Den Bosch, S. F. Koelewijn, G. T. Beckham and B. F. Sels, *Chem. Soc. Rev.*, 2018, **47**, 852–908.
24 R. Ma, M. Guo and X. Zhang, *ChemSusChem*, 2014, **7**, 412–415.
25 B. Huskinson, M. P. Marshak, C. Suh, S. Er, M. R. Gerhardt, C. J. Galvin, X. Chen, A. Aspuru-Guzik, R. G. Gordon and M. J. Aziz, *Nature*, 2014, **505**, 195–198.
26 Y. Hu, S. Li, X. Zhao, C. Wang, X. Zhang, J. Liu, L. Ma, L. Chen and Q. Zhang, *Catal. Commun.*, 2022, **172**, 106532.
27 S. R. Pradhan, M. Paszkiewicz-Gawron, D. Łomot, D. Lisovytskiy and J. C. Colmenares, *Molecules*, 2022, **27**(24), 8731.
28 S. Sutradhar, N. Alam, L. P. Christopher and P. Fatehi, *Catal. Today*, 2022, **404**, 49–62.
29 H. Y. Shin, S. M. Jo and S. S. Kim, *Ind. Crops Prod.*, 2022, **187**, 115539.
30 J. F. Kadla, H. M. Chang and H. Jameel, *Holzforschung*, 1999, **53**, 277–284.
31 Q. Xiang and Y. Y. Lee, *Appl. Biochem. Biotechnol., Part A*, 2000, **84–86**, 153–162.
32 P. Chow, G. L. Rolfe and W. Motter, *Wood Fiber Sci.*, 1995, **27**, 319–326.
33 K. S. Suslick, Y. Didenko, M. M. Fang, T. Hyeon, K. J. Kolbeck, W. B. McNamara III, M. M. Mdleleni and M. Wong, *Philos. Trans. R. Soc., A*, 1999, 335–353.
34 I. A. Gilca, V. I. Popa and C. Crestini, *Ultrason. Sonochem.*, 2015, **23**, 369–375.
35 Z. Zhang, V. Terrasson and E. Guénin, *Nanomaterials*, 2021, **11**, 1336.
36 P. K. Mishra and R. Wimmer, *Ultrason. Sonochem.*, 2017, **35**, 45–50.
37 S. B. Kristensen, T. van Mourik, T. B. Pedersen, J. L. Sørensen and J. Muff, *Sci. Rep.*, 2020, **10**, 1–10.
38 A. Khetan, *Batteries*, 2023, **9**, 24.
39 T. Sun, W. Zhang, Q. Nian and Z. Tao, *Nano-Micro Lett.*, 2023, **15**, 1–14.
40 Y. Ding, L. Xie, Y. Zhang, X. Chen, Y. Niu, J. Xu, Q. Han, X. Qiu, Y. Miao, Y. Xiao, L. Zhu and X. Cao, *J. Electroanal. Chem.*, 2023, **928**, 117054.
41 J. Adamcyk, S. Beisl, S. Amini, T. Jung, F. Zikeli, J. Labidi and A. Friedl, *Polymer*, 2021, **13**, 1–13.
42 S. Beisl, A. Friedl and A. Miltner, *Int. J. Mol. Sci.*, 2017, **18**(17), 2367.
43 M. Witzler, A. Alzagameem, M. Bergs, B. El Khaldi-Hansen, S. E. Klein, D. Hielscher, B. Kamm, J. Kreyenschmidt, E. Tobiasch and M. Schulze, *Molecules*, 2018, **23**, 1–22.
44 A. K. Gupta, S. Mohanty and S. K. Nayak, *Mater. Focus*, 2015, **3**, 444–454.
45 R. Ma, M. Guo and X. Zhang, *Catal. Today*, 2018, **302**, 50–60.
46 G. Gellerstedt, R. Agnemo and G. Gellerstedt, *Acta Chem. Scand.*, 1980, 337–342.
47 L. D. Antonino, J. R. Gouveia, R. R. de Sousa Júnior, G. E. S. Garcia, L. C. Gobbo, L. B. Tavares and D. J. Dos Santos, *Molecules*, 2021, **26**, 1–12.
48 B. Ramakoti, H. Dhanagopal, K. Deepa, M. Rajesh, S. Ramaswamy and K. Tamilarasan, *Bioresour. Technol. Rep.*, 2019, **7**, 100293.
49 N. Izaguirre, E. Robles, R. Llano-Ponte, J. Labidi and X. Erdocia, *Ind. Crops Prod.*, 2022, **175**, 114251.
50 A. Rawle, *Adv. Colour Sci. Technol.*, 2002, **5**, 1–12.
51 Z. H. Liu, N. Hao, S. Shinde, M. L. Olson, S. Bhagia, J. R. Dunlap, K. C. Kao, X. Kang, A. J. Ragauskas and J. S. Yuan, *ACS Sustainable Chem. Eng.*, 2019, **7**, 2634–2647.
52 M. Österberg, M. H. Sipponen, B. D. Mattos and O. J. Rojas, *Green Chem.*, 2020, **22**, 2712–2733.
53 A. Hulsmans, K. Joris, N. Lambert, H. Rediers, P. Declerck, Y. Delaedt, F. Ollevier and S. Liers, *Ultrason. Sonochem.*, 2010, **17**, 1004–1009.
54 Y. Chen, K. Zheng, L. Niu, Y. Zhang, Y. Liu, C. Wang and F. Chu, *Int. J. Biol. Macromol.*, 2019, **128**, 414–420.
55 A. Sluiter, B. Hames, R. Ruiz, C. Scarlata, J. Sluiter, D. Templeton and D. Crocker, *Determination of structural carbohydrates and lignin in Biomass-Laboratory Analytical Procedure (LAP)*, 2012.
56 F. F. De Menezes, G. J. M. De Rocha and R. M. Filho, *Chem. Eng. Trans.*, 2016, **50**, 397–402.
57 A. Guerra, I. Filpponen, L. A. Lucia and D. S. Argyropoulos, *J. Agric. Food Chem.*, 2006, **54**, 9696–9705.
58 A. A. Myint, H. W. Lee, B. Seo, W. S. Son, J. Yoon, T. J. Yoon, H. J. Park, J. Yu, J. Yoon and Y. W. Lee, *Green Chem.*, 2016, **18**, 2129–2146.
59 A. García, M. González Alriols, G. Spigno and J. Labidi, *Biochem. Eng. J.*, 2012, **67**, 173–185.
60 W. Wu, T. Liu, X. Deng, Q. Sun, X. Cao, Y. Feng, B. Wang, V. A. L. Roy and R. K. Y. Li, *Int. J. Biol. Macromol.*, 2019, **126**, 1030–1036.
61 X. Meng, C. Crestini, H. Ben, N. Hao, Y. Pu, A. J. Ragauskas and D. S. Argyropoulos, *Nat. Protoc.*, 2019, **14**, 2627–2647.
62 H. Li, Y. Deng, J. Liang, Y. Dai, B. Liu, Y. Ren, X. Qiu and C. Li, *BioResources*, 2016, **11**, 3073–3083.